Formation of a Massive Lenticular Galaxy Under the Tidal Interaction with a Group of Dwarf Galaxies

Downloaded from: https://research.chalmers.se, 2025-12-09 23:30 UTC

Citation for the original published paper (version of record):
Xu, J., Zhu, M., Hess, K. et al (2023). Formation of a Massive Lenticular Galaxy Under the Tidal Interaction with a Group of Dwarf
Galaxies. Astrophysical Journal Letters, 958(2). http://dx.doi.org/10.3847/2041-8213/ad0cf5

N.B. When citing this work, cite the original published paper.

research.chalmers.se offers the possibility of retrieving research publications produced at Chalmers University of Technology. It covers all kind of research output: articles, dissertations, conference papers, reports etc. since 2004. research.chalmers.se is administrated and maintained by Chalmers Library

(article starts on next page)

The Astrophysical Journal Letters, 958:L31 (11pp), 2023 December 1 https://doi.org/10.3847/2041-8213/ad0cf5
© 2023. The Author(s). Published by the American Astronomical Society.
OPEN ACCESS

Formation of a Massive Lenticular Galaxy Under the Tidal Interaction with a Group of Dwarf Galaxies

Jin-Long Xu[1,2,3], Ming Zhu[1,2,3], Kelley M. Hess[4], Naiping Yu[1,2,3], Chuan-Peng Zhang[1,2,3], Xiao-Lan Liu[1,2,3], Mei Ai[1,2,3], Peng Jiang[1,2,3], and Jie Wang[1]
[1] National Astronomical Observatories, Chinese Academy of Sciences, Beijing 100101, People's Republic of China; xujl@bao.ac.cn
[2] Guizhou Radio Astronomical Observatory, Guizhou University, Guiyang 550000, People's Republic of China
[3] CAS Key Laboratory of FAST, National Astronomical Observatories, Chinese Academy of Sciences, Beijing 100101, People's Republic of China
[4] Department of Space, Earth and Environment, Chalmers University of Technology, Onsala Space Observatory, 43992 Onsala, Sweden
Received 2023 October 17; revised 2023 November 9; accepted 2023 November 16; published 2023 November 29

Abstract

Based on the atomic-hydrogen (H I) observations using the Five-hundred-meter Aperture Spherical radio Telescope, we present a detailed study of the gas-rich massive S0 galaxy NGC 1023 in a nearby galaxy group. The presence of a H I extended warped disk in NGC 1023 indicates that this S0 galaxy originated from a spiral galaxy. The data also suggest that NGC 1023 is interacting with four dwarf galaxies. In particular, one of the largest dwarf galaxies has fallen into the gas disk of NGC 1023, forming a rare bright–dark galaxy pair with a large gas clump. This clump shows the signature of a galaxy but has no optical counterpart, implying that it is a newly formed starless galaxy. Our results first suggest that a massive S0 galaxy in a galaxy group can form via the morphological transformation from a spiral under the joint action of multiple tidal interactions.

Unified Astronomy Thesaurus concepts: Galaxy evolution (594); Galaxy formation (595)

1. Introduction

One of the biggest challenges for extragalactic astrophysics is to figure out how different types of galaxies are formed. Lenticular (S0) galaxies, located between ellipticals and spirals on the Hubble sequence, are composed of a central bulge and a stellar disk without spiral arms. Two main formation pathways for S0 galaxies have been identified, either as fading spirals or as the result of galaxy mergers (Fraser-McKelvie et al. 2019; Deeley et al. 2020, 2021). However, recent observations have demonstrated that S0 galaxies form a diverse population (Coccato et al. 2020), so there are other plausible mechanisms for their formation that still need to be probed.

It has been suggested that S0 galaxies descended from spirals through morphological transformation (Dressler 1980; Laurikainen et al. 2010; Rizzo et al. 2018). Some dynamic processes may deplete the gas of the spirals and stop their star formation (Larson et al. 1980). Different processes would have different effects on the stellar and gas kinematics in S0 galaxies. The stellar kinematics have mostly been probed using spatially resolved stellar or globular cluster distributions (Herrmann & Ciardullo 2009; Zanatta et al. 2018). Simulations indicate that the stellar kinematics have a velocity dispersion as high or even higher than rotational velocity, if the S0 galaxies are the result of merger events (Bournaud et al. 2005). In the scenario of a fading spiral, the gas in the spiral arms is stripped by environmental mechanisms such as ram pressure stripping, harassment, or starvation (Gunn et al. 1972; Moore et al. 1998; Balogh et al. 2000). These relatively gentle gas-stripping processes should not have a significant impact on the stellar kinematics of the spirals, which would lead to a rotation that would dominate the disks of the S0 galaxies (Coccato et al. 2020; Deeley et al. 2020).

Original content from this work may be used under the terms of the Creative Commons Attribution 4.0 licence. Any further distribution of this work must maintain attribution to the author(s) and the title of the work, journal citation and DOI.

The NGC 1023 group is one of the most extensively studied nearby galaxy groups. Optical observations toward the group have detected dozens of dwarf galaxies (Trentham & Tully 2009). The massive S0 galaxy NGC 1023 is the brightest member of this group at a distance of 10.4 Mpc (Tonry et al. 2001; Cappellari et al. 2011; Dolfi et al. 2021). The gas content of early-type galaxies is often thought to be insignificant. NGC 1023 is one of the nearest members of the rare class of H I-rich S0 galaxies, making it an ideal laboratory to test a massive S0 galaxy formation within a galaxy group. NGC 1023 has a complex set of substructures, including a young (3.4 Gyr) and metal-rich ([Fe/H] = 0.50 dex) nuclear disk and a faster bar (Debattista et al. 2002; Corsini et al. 2016). Deep H I observations from the Westerbork Synthesis Radio Telescope (WSRT) showed that NGC 1023 has an extended and complex gas distribution (Sancisi et al. 1984; Morganti et al. 2006). Within the innermost part of the NGC 1023 group, there are four late-type dwarf companion galaxies (Trentham & Tully 2009), called NGC 1023A, NGC 1023B, NGC 1023C, and NGC 1023D. Only NGC 1023A was considered to be an ongoing interaction with the main galaxy NGC 1023 and it has been stripped of its gas (Capaccioli et al. 1986; Dolfi et al. 2021; de Brito Silva et al. 2022), resulting in an extended and irregular H I distribution detected in NGC 1023.

The kinematics of stars, globular clusters (GCs), and planetary nebulae (PNe) in NGC 1023 imply that its stellar disk is rotationally supported at small radii ($V_{\rm rot}/\sigma > 1$), while more pressure is supported at large radii ($V_{\rm rot}/\sigma < 1$) (Noordermeer et al. 2008; Dolfi et al. 2021). Here $V_{\rm rot}$ and σ represent rotation velocity and velocity dispersion. Furthermore, the peak $V_{\rm rot}/\sigma$ in its stellar disk is greater than 4 (Noordermeer et al. 2008; Cortesi et al. 2011, 2013, 2016), which is higher than that ($1 < V_{\rm rot}/\sigma \leqslant 2$) of minor mergers ($3 <$ mass ratio <10) and that ($V_{\rm rot}/\sigma < 1$) of major mergers (mass ratio <3) (Bournaud et al. 2005), but lower than the one expected for spiral galaxies (Herrmann & Ciardullo 2009). Both the fading spiral and merger scenarios appear to be

inconsistent with the observed stellar kinematics of NGC 1023. Moreover, considering a lower luminosity of NGC 1023A relative to NGC 1023 (Capaccioli et al. 1986; Noordermeer et al. 2008), NGC 1023A is not sufficiently massive to cause a strong morphological response in NGC 1023. H I gas emission is typically more extended than stars in the outer parts of the galaxy. H I observations can be considered as an excellent tool to investigate S0 galaxy formation.

1.1. Observations and Data Reduction

Using the Five-hundred-meter Aperture Spherical radio Telescope (FAST) in 2021 December (Jiang et al. 2019, 2020), we performed a $2^\circ \times 2^\circ$ mapping observation of H I (1420.4058 MHz) toward S0 galaxy NGC 1023. The mapping observation used the Multi-beam on-the-fly (OTF) mode. This mode is designed to map the sky with 19 beams simultaneously and has a similar scanning trajectory. Furthermore, we set the scan velocity as $15'' \ s^{-1}$ and an integration time of 1 s per spectrum. It formally works in the frequency range from 1050 to 1450 MHz. We used the digital Spec(W) backend, which has a bandwidth of 500 MHz and 64k channels, resulting in a frequency resolution of 7.629 kHz and corresponding to a velocity resolution of 1.6 $km\,s^{-1}$. For intensity calibration to antenna temperature (T_A), a noise signal with an amplitude of 10 K was injected in a period of 32 s. The half-power beamwidth is $\sim 2\farcm9$ at 1.4 GHz for each beam. The pointing accuracy of the telescope was better than $10''$. To improve sensitivity, we observed two times for the NGC 1023 region, using a total of 2.3 hr. The system temperature was around 25 K during the observations. The detailed data reduction is similar to Xu et al. (2021). Using the ArPLS algorithm (Baek et al. 2015), we mitigated radio frequency interference by a fitting procedure of the data in the time-frequency domain. Finally, we made the calibrated data into the standard cube data, with a pixel of $1\farcm0 \times 1\farcm0$. A gain T_A/S_ν has been measured to be about 15 K Jy^{-1}, while a measured relevant main beam gain T_B/S_ν is about 20 K Jy^{-1} at 1.4 GHz for each beam, where T_B is the brightness temperature. To construct a highly sensitive H I image, the velocity resolution of the FAST data is smoothed to $\sim 3.2\ km\,s^{-1}$. The mean noise rms in the observed image is ~ 1.3 mJy $beam^{-1}$ in the observed region.

In addition, Digitized Sky Survey (DSS) Blue-band and GALEX near-ultraviolet (NUV) and far-ultraviolet (FUV) data are available at NASA/IPAC Extragalactic Database.[5] The Hubble Space Telescope (HST) data are publicly available at Hubble Legacy Archive.[6]

2. Results

We have performed deeper mapping observations of the H I emission toward NGC 1023 using the FAST. The final data cube had an rms noise level of 1.3 mJy $beam^{-1}$ in the line channels, corresponding to a column density of $1.5 \times 10^{17}\ cm^{-2}\ channel^{-1}$ at a velocity resolution of $\sim 3.2\ km\ s^{-1}$. We found that the H I gas emission associated with NGC 1023 is mainly located within the redshift velocity range of 406.0–972.0 $km\,s^{-1}$. Relative to the systemic velocity (615 $km\,s^{-1}$) of NGC 1023 (Capaccioli et al. 1986), such velocity ranges from −210 to 356 $km\,s^{-1}$. Based on the velocity range, we constructed a H I column-density map of NGC 1023, as shown in Figure 1(a). The column-density error on the map is $1\sigma = 1.3 \times 10^{18}\ cm^{-2}$, which is about 1 order of magnitude lower than that from the WSRT observation for NGC 1023 (Sancisi et al. 1984; Morganti et al. 2006). Our high-sensitivity observations of the H I gas emission in NGC 1023 show a very extended and unbroken structure. NGC 1023 is almost in the center of the extended structure. In Figure 1(b), the H I velocity map of the extended structure shows a clear gradient from southwest to northeast. We infer that the extended structure is a rotating gas disk of NGC 1023. As depicted by a dotted line in Figure 1(b), the gas disk is twisty, and the rotation axis of the gas disk is misaligned with the photometric axis, but it almost matches the bar direction of NGC 1023 (Bettoni et al. 2000; Debattista et al. 2002).

The gas disk of NGC 1023 in Figure 1(a) also exhibits an asymmetric outskirts, involving two striking tails (tail NE and tail SE). The tail SE was detected for the first time in NGC 1023 based on our higher-sensitivity H I observations. Since no nearby massive galaxies were detected in the direction of the tail SE, this tail cannot be a tidal tail that was dragged out by a galaxy outside NGC 1023. Both the velocity maps of the tail NE and tail SE in Appendix A show a gradient toward the center of NGC 1023. Moreover, the asymmetric outskirts of NGC 1023 connect two dwarf galaxies (NGC 1023C and NGC 1023D), whereas dwarf galaxies NGC 1023A and NGC 1023B appear to be embedded in the gas disk of NGC 1023. Figure 2 shows the H I column-density map of each dwarf galaxy. We found that NGC 1023B, NGC 1023C, and NGC 1023D, respectively, connected with a part of the gas disk of NGC 1023 by a bridge. The simulations show that when two galaxies interact, they will result in tidal tails in each galaxy (Toomre & Toomre 1972; Springel et al. 2005). In particular, they will form a connecting bridge, which could provide the most direct evidence that two galaxies are interacting. The bending of the tail NE toward NGC 1023C indicates that this tail may have formed because of a tidal effect from this dwarf galaxy. We estimated that the ratio (M_{dyn}/M_{bar}) of the dynamical masses to the baryons masses is ∼11.5 for NGC 1023C (See Appendix D). From previous observations and numerical simulations, $M_{dyn}/M_{bar} \simeq 1$ is a characteristic of tidal dwarf galaxies (Duc et al. 2004; Bournaud & Duc 2006; Lelli et al. 2015). Both the NGC 1023B and NGC 1023D are similar in kinematics to the NGC 1023C. We suggest that these three dwarf galaxies are interacting with NGC1023, not the tidal dwarf galaxies that formed when galaxies merged.

To analyze the kinematics of NGC 1023 in velocity space, we created velocity and position (PV) diagrams through its center with a half-beamwidth and a length of 21′. The cutting directions start from the north and run counterclockwise every 15°. From the PV diagrams in Appendix B, we found that NGC 1023 shows a rotational gas disk that hosts several gas clumps. In the highest column-density region of the gas disk, we identified a pair of gas clumps, as indicated by the blue boxes. To illustrate the identified pair system, we made a special PV diagram with a cutting direction along the connecting axis of the pair members. The identified pair is highlighted by a cyan dashed box in Figure 3(a). The spectroscopic observations indicate that the heliocentric radial velocity of NGC 1023 is $615 \pm 20\ km\,s^{-1}$, whereas that of NGC 1023A is $742 \pm 30\ km\,s^{-1}$. By comparing these velocities to the PV diagram in

[5] http://ned.ipac.caltech.edu/
[6] https://hla.stsci.edu/

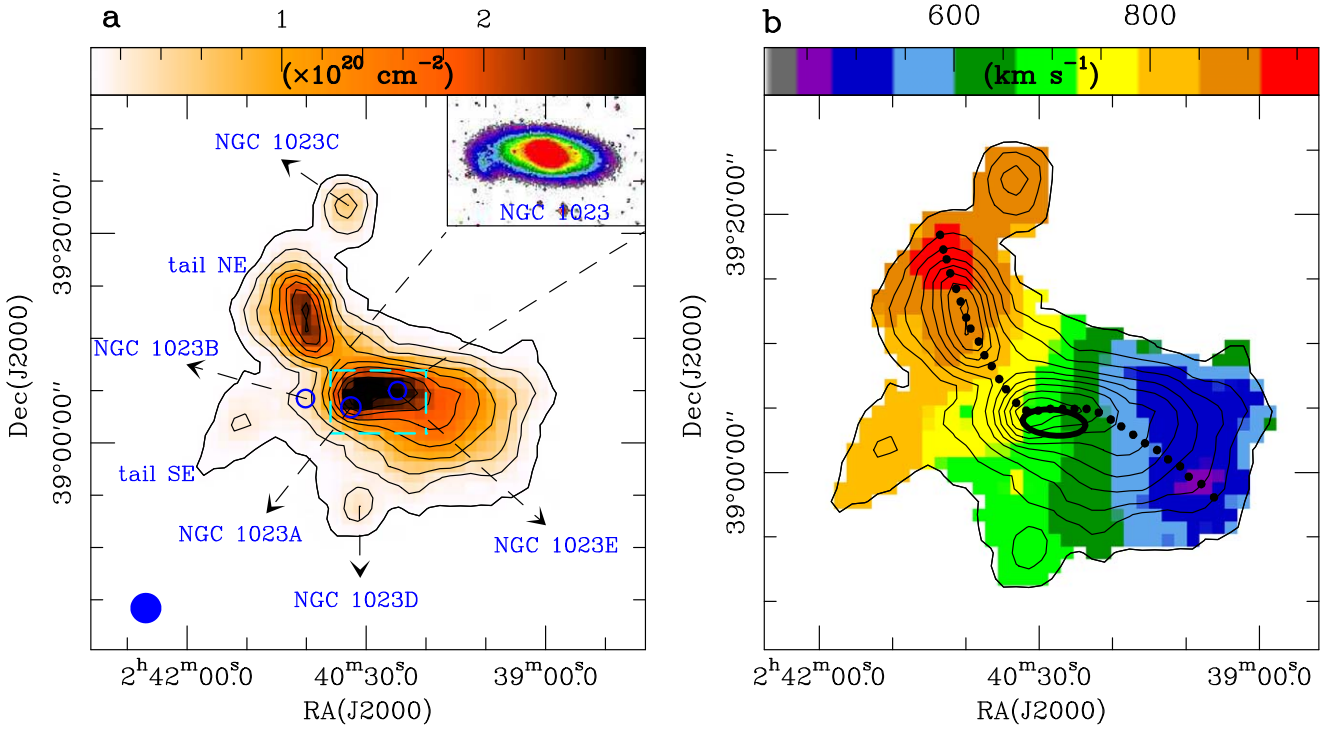

Figure 1. Overview of the new H I observations of NGC 1023. (a) H I column-density map shown in color scale and black contours. The black contours begin at 4.0×10^{18} cm^{-2} (3σ) in steps of 3.9×10^{19} cm^{-2}. The Digitized Sky Survey (DSS) *B*-band image of NGC 1023 is shown in the top-right corner, while the FAST beam in a green filled circle is shown in the bottom-left corner. (b) H I velocity field (moment 1) map in color scale overlaid with the H I column-density in the black contours. These velocities are relative to the systemic velocity (615 km s^{-1}) of NGC 1023. The black ellipse indicates the position and size of NGC 1023. We use a dotted line to indicate the velocity gradient. This dotted line roughly follows the main axis of H I complex of NGC 1023.

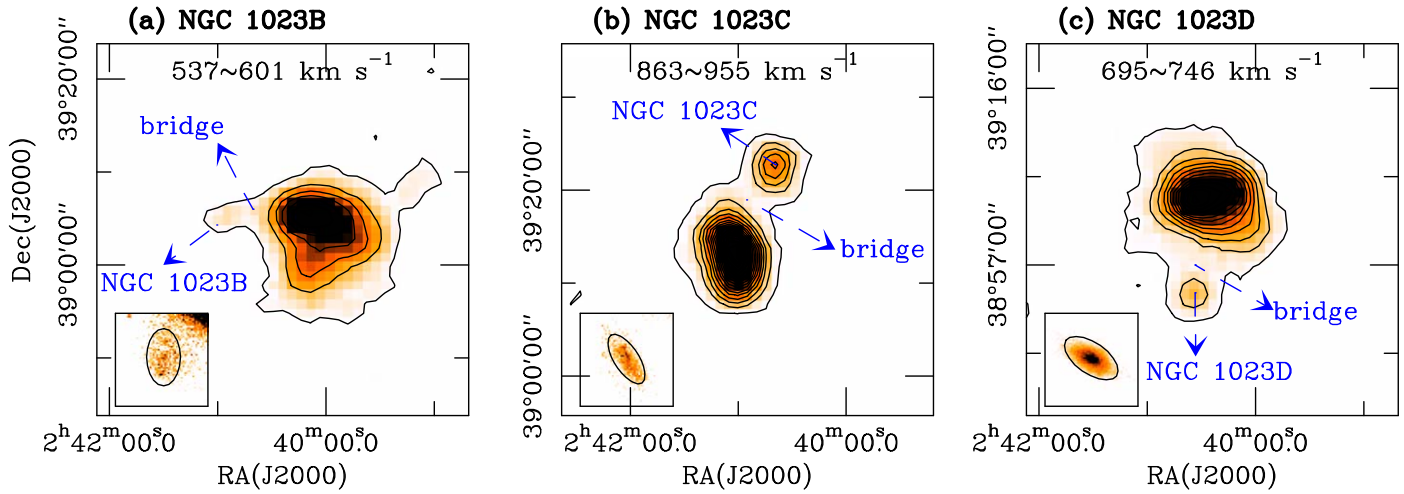

Figure 2. Three dwarf galaxies interacting with NGC 1023. The H I column-density map of each dwarf galaxy is shown in color scale and black contours, while the Pan-STARRS1 g-band image is shown in the lower-left corner of each panel. The H I column density in each panel was created within a certain integrated-velocity range around each dwarf galaxy. Relative to the systemic velocity (615 km s^{-1}) of NGC 1023, the integrated-velocity range for each dwarf galaxy is also presented in the top of each panel, while the black contours begin at 3.3×10^{18} cm^{-2} in steps of 1.2×10^{19} cm^{-2} in each panel.

Figure 3(a), we found that one member of the pair is associated with NGC 1023A, and the other is a newly discovered H I clump, named NGC 1023E. We used the Source Finding Application (SoFiA2) pipeline (Westmeier et al. 2021) to determine the radial velocity and coordinate position of NGC 1023E. By comparing these systemic velocities, NGC 1023E with a radial velocity of 704.2 ± 1.6 km s^{-1} seems to be located between NGC 1023 and NGC 1023A in the line of sight.

NGC 1023A and NGC 1023E in Figure 3(a) are connected not only in space but also in velocity, implying that there is a H I gaseous bridge between them. Moreover, both the dense gases within NGC 1023A and NGC 1023E show a bowed head-tail structure in the column-density maps of Figure 3(b). Figure 4(a) shows the overlapping maps of the dense regions of NGC 1023A and NGC 1023E. We found that the orientation of these identified tails is not random. The tail of NGC 1023A bends toward the head of NGC 1023E. Similarly, the tail of

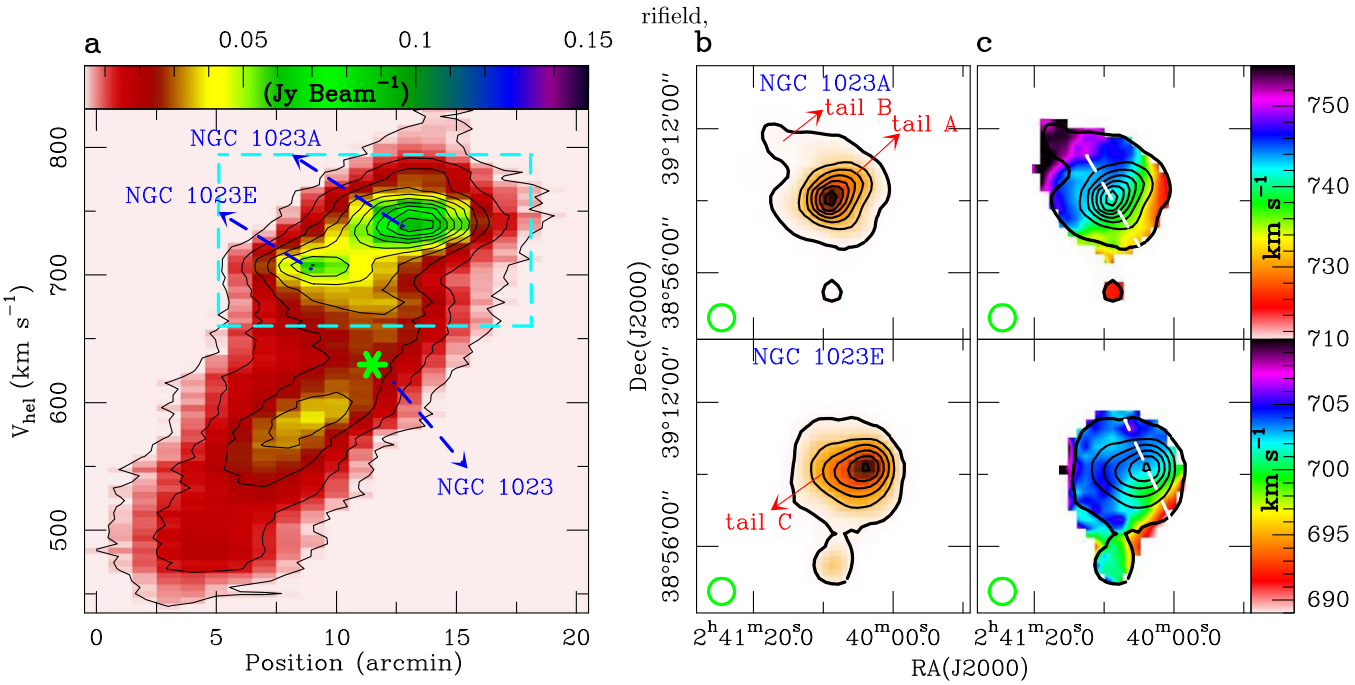

Figure 3. A galaxy pair within the gas disk of NGC 1023. (a) Position–velocity (PV) diagram in color scale overlaid with black contours. The black contours begin at 3σ ($1\sigma = 1.3$ mJy beam^{-1}) in steps of 7σ. We use a cyan dashed box to mark the galaxy pair in the PV diagram. (b) and (c) H I column-density and velocity-field maps. The black contours begin at 3.0×10^{18} cm^{-2} in steps of 1.8×10^{19} cm^{-2} in each panel. The white dashed line in each velocity-field map marks the direction of the velocity gradient. These velocities are relative to the systemic velocities of NGC 1023A and NGC 1023E, respectively. The FAST beam in green circle is shown in the bottom-left corner of each panel. We adopted the integrated-velocity range from 108.2 to 147.5 km s^{-1} for NGC 1023A, and from 73.7 to 108.2 km s^{-1} for NGC 1023E.

NGC 1023E bends toward the head of NGC 1023A. In order to confirm whether these are true tidal tails, we also made a PV diagram with the cutting direction shown in Figure 4(a). The PV diagram in Figure 4(b) makes the bowed head-tail structures in NGC 1023A and NGC 1023E more obvious. And both tails are high speed relative to their central dense cores. It closely resembles the traits of the tidal tail. The bridge and tidal tails detected in the pair system imply that NGC 1023A and NGC 1023E are interacting. Furthermore, as shown in Figure 4(a), previously identified blue faint fuzzies (FFs) with a few 100 Myr coincide well with the interacting system in spatial distribution (Forbes et al. 2014). The FFs are a relatively new class of star cluster. Furthermore, two blue clusters with ages between 125 and 500 Myr are identified in NGC 1023A on the basis of their strong Balmer lines (Larsen & Brodie 2002). The enhanced star formation activity in NGC 1023A further confirmed that NGC 1023A is interacting with NGC 1023.

The formation of a pair system with the dwarf galaxy NGC 1023A suggests that NGC 1023E is probably not a simple gas clump. In Figure 3(c), the moment 1 maps of both NGC 1023A and NGC 1023E show a relatively regular velocity gradient, which is regarded to be a key characteristic of galaxies. In order to verify the existence of the velocity gradients in NGC 1023A and NGC 1023E, we made the new PV diagrams along their velocity gradients, denoted by the white dashed lines visible in Figure 3(c). The PV diagrams in Figure 8 confirm that both NGC 1023A and NGC 1023E have a velocity gradient. Additionally, we estimated the H I gas masses ($M_{\rm HI}$) of NGC 1023A and NGC 1023E to be $2.7^{+0.3}_{-0.3} \times 10^8\ M_\odot$ and $2.0^{+0.2}_{-0.2} \times 10^8\ M_\odot$, and their effective radius to be 20.0 ± 0.4 kpc and 18.7 ± 0.4 kpc, respectively, indicating that NGC 1023E has a similar size and H I masses with NGC 1023A. Furthermore, both the $M_{\rm dyn}/M_{\rm bar}$ are ~5.5, which indicates that the dark matter dominates in NGC 1023A and NGC 1023E. All of this evidence suggests that NGC 1023E can be classified as a galaxy, like NGC 1023A.

In order to investigate the presence of stellar components that could be associated with NGC 1023E, we used HST g and z bands, and GALEX NUV and FUV images. Previous studies established a strong correlation between the H I mass ($M_{\rm HI}$) and the optical disk diameter (D_{25}) in kiloparsecs for late-type galaxies, as shown by the equation $\log M_{\rm HI} = a + b \times \log D_{25}$, where the coefficients could be adopted by $a = 7.0$ and $b = 1.95$ (Broeils & Rhee 1997; Toribio et al. 2011). We can make the restriction on the scales of potential optical emission from NGC 1023E using the correlation. Finally, the predicted values for D_{25} are 5.4 ± 0.6 kpc for NGC 1023A and 4.7 ± 0.5 kpc for NGC 1023E. As seen in Figure 5, the optical emission of NGC 1023A is just within the predicted optical scale. But for NGC 1023E, we did not detect any extended optical or ultraviolet (UV) emission in the predicted radius of NGC 1023E, except for a foreground star with a parallax of 0.76 ± 0.08 mas, which is identified by using the Gaia star diagram (Gaia Collaboration et al. 2016).

3. Discussions and Summary

Neither the fading spirals nor the result of galaxy mergers can explain the stellar kinematics of NGC 1023, implying that it is necessary to explore other mechanisms for the formation of this S0 galaxy. From our highly sensitive H I observations, NGC 1023 clearly displays an extended warped gas disk. We obtained that the total mass of the gas disk is about $2.0 \times 10^9 M_\odot$ (See Appendix C). It was previously thought

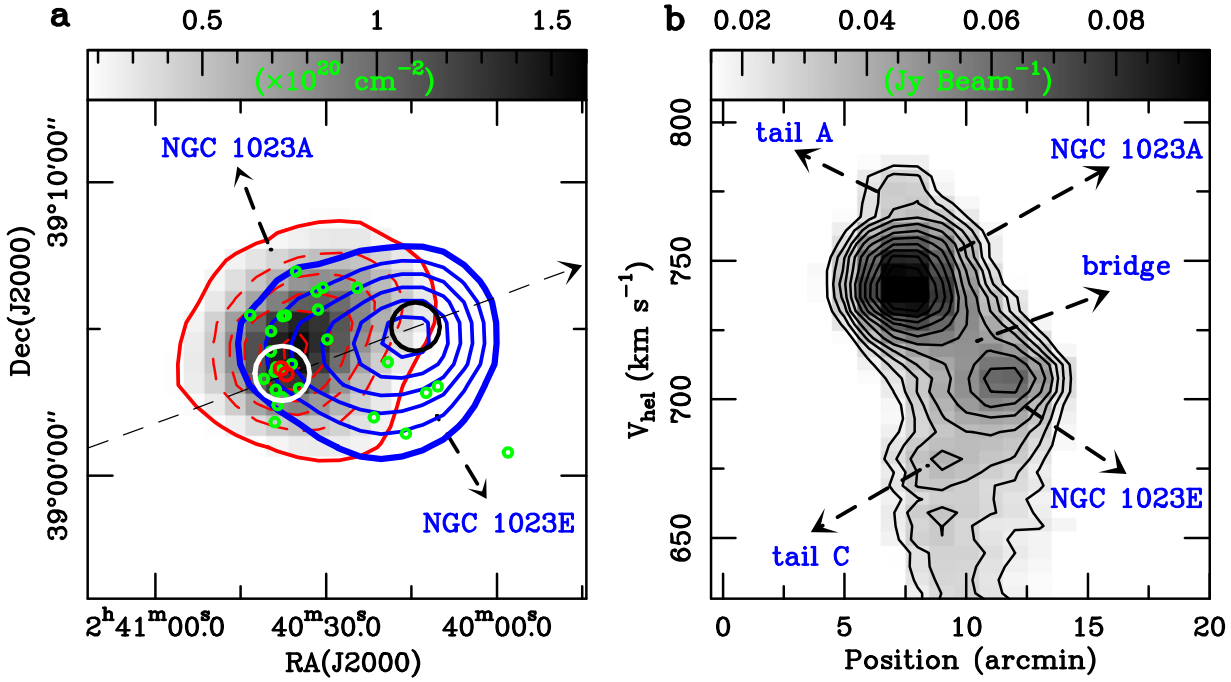

Figure 4. Morphology of the galaxy pair. (a) The H I column-density maps of the dense regions of NGC 1023A (red contours and black scale) and NGC 1023E (blue contours). Both blue and red contours begin at 2.0×10^{19} cm^{-2}. The white circle represents the predicted optical radius of NGC 1023A, while the black circle represents the predicted optical radius of NGC 1023E. Previously identified blue faint fuzzies (FFs; Forbes et al. 2014) and two stellar clusters (Larsen & Brodie 2002) are indicated by the green and red circles, respectively. (b) PV diagram in black scale overlaid with black contours. The cutting direction is shown in a black arrow in panel (a). The black contours begin at 20σ ($1\sigma = 1.3$ mJy beam^{-1}) in steps of 4σ.

that the irregular H I gas detected in NGC 1023 was stripped gas from its companion NGC 1023A (Cortesi et al. 2016; Dolfi et al. 2021). We observed that NGC 1023A is still a gas-rich dwarf galaxy (See Figure 3(b)), and thus excluded the possibility that the H I gas in NGC 1023 is donated by this companion. In addition, H I observations of galaxies in the local Universe have indicated that extended warped disks are usually related to spiral galaxies (Briggs 1990; García-Ruiz et al. 2002). The warps are thought to originate from interactions with nearby galaxies and cold-mode accretion (Sancisi et al. 2008; van der Kruit & Freeman 2011; Rahmani et al. 2018). In this study, we found that NGC 1023 is interacting with four dwarf galaxies. The largest galaxy (NGC 1023A) among them seems to have fallen into the gas disk of NGC 1023, forming a bright–dark galaxy pair. This strongly supports that the warped gas disk of NGC 1023 originated from interactions. The warped gas disk could be a fossil record of the progenitor galaxy of NGC 1023. This result may favor a model in which NGC 1023 formed from a spiral by tidal interactions.

Tidal interaction is also considered as a possible physical mechanism for the transformation of spirals into S0 galaxies in galaxy groups from the chemodynamical simulations (Bekki & Couch 2011). The simulated S0 galaxies transformed from spirals in this mechanism have young and metal-rich stellar populations in their bulges. The simulated S0 galaxies have a lower rotation amplitude ($V_{\rm rot}/\sigma \sim 1$) and a flatter radial velocity-dispersion profile. The cold H I gas adjacent to the simulated S0 galaxies presents unique spatial distributions, such as rings, long tails, and massive H I clouds without optical counterparts. NGC 1023 has a nuclear disk, which is characterized by a younger (∼3.4 Gyr) and more metal-rich ([Fe/H] = 0.50 dex) stellar population in its bulge (Corsini et al. 2016). The stellar and GCs/PNe kinematics reveal that NGC 1023 is more pressure-supported at its large optical radii ($V_{\rm rot}/\sigma < 1$), and has relatively flatter profiles in its radial velocity dispersion (Noordermeer et al. 2008; Dolfi et al. 2021). In particular, the gas disk of NGC 1023 has two long tails (tail NE and tail SE) and a H I gas clump without an optical counterpart (NGC 1023E). The same chemical, kinematical, and structural properties in NGC 1023 as in the simulated S0s suggest that NGC 1023 is formed via the morphological transformation from a spiral under the tidal interactions. However, there is a difference that NGC 1023 is a gas-rich S0 galaxy, while the simulated S0 galaxies end up being gas-poor. This may be due to the fact that the simulated S0 galaxies are interacting with other similarly massive or more massive galaxies within the group (Bekki & Couch 2011), while in NGC 1023 the interactions are with a number of dwarf galaxies. The relatively strong interactions with massive galaxies may strip away gas from the predecessor of the S0 galaxy.

The previous model predicted that the majority of gas in galaxies with baryonic masses more than $10^9\ M_\odot$ will become Toomre unstable and result, inevitably, in star formation (Taylor & Webster 2005). The formed NGC 1023 is a gas-rich S0 galaxy with a H I mass of $2.0 \times 10^9 M_\odot$. We also obtained that the peak column density is $\sim 3.3 \times 10^{20}$ cm^{-2} in its gas disk of NGC 1023, which is slightly less than that of 5.0×10^{20} cm^{-2} from the WSRT observation. The peak value is near the column-density threshold (5.0×10^{20} cm^{-2}) for star formation (Gallagher & Duc 1984; Davies et al. 2006). This suggests that although there is a significant amount of cold gas in NGC 1023, the forming star in the cold gas has been suppressed. The quenching of the forming star in NGC 1023 is not due to a lack of gas but is likely to be caused by the external tidal effect.

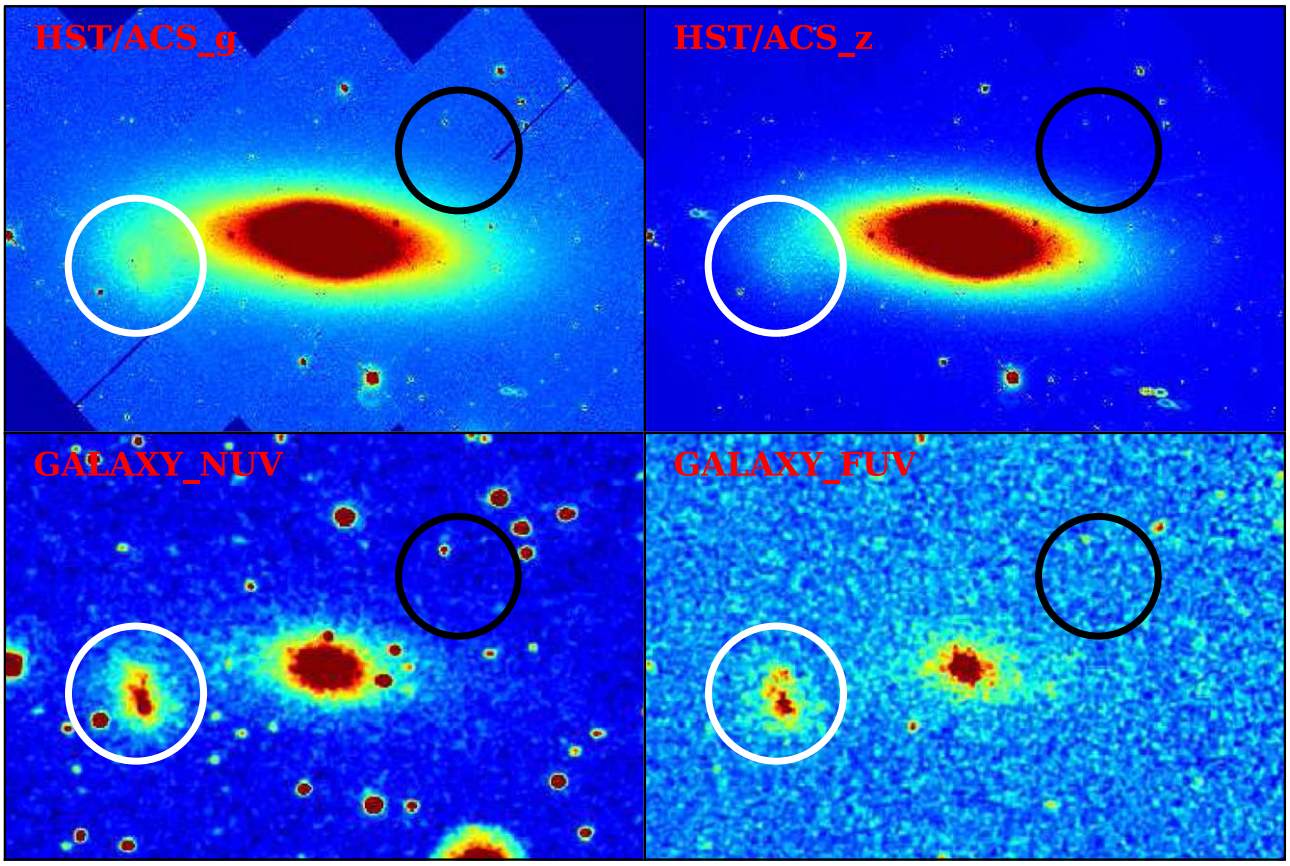

Figure 5. Optical and ultraviolet (UV) emission maps of the galaxy pair members. The Hubble Space Telescope (HST) g and z bands data are used to trace the optical emission, and the GALEX NUV and FUV data for the UV emission. Fluxes in each band are on an arbitrary unit. The white circle represents the predicted optical radius of NGC 1023A, while the black circle represents the predicted optical radius of NGC 1023E.

For the formation of S0 galaxies due to the tidal-interaction mechanism, it can create large H I gas clumps from the gas stripped from spirals being transformed into the S0 galaxies (Bekki & Couch 2011). If the clump is self-gravitating, it could become a small dwarf galaxy that also retains little dark matter from its parents' haloes (Barnes & Hernquist 1992). We also detected a large gas clump NGC 1023E with a H I mass of approximately $2.0 \times 10^8 M_\odot$ in the gas disk of NGC 1023. NGC 1023E shares the same morphology and dynamics as dwarf galaxy NGC 1023A. Furthermore, it can be observed that the H I gas present in NGC 1023E can be simulated as a rotating gas disk (as outlined in Appendix D). Therefore, NGC 1023E has all the characteristics of a galaxy but no optical counterpart from the deep HST observations. The dominant presence of dark matter ($M_{\rm dyn}/M_{\rm bar} \simeq 5$) in NGC 1023E suggests that it is likely to be a newly formed starless galaxy, rather than a tidal dwarf galaxy, which is generally located in tidal tails and in the absence of dark matter ($M_{\rm dyn}/M_{\rm bar} \simeq 1$) (Lelli et al. 2015). Based on the HST g-band image, we estimated that the upper limit surface brightness of NGC 1023E is $\mu_g = 33.8$ mag arcsec^{-2}.

In sum, for the first time in observations, we have confirmed that a massive S0 galaxy in a galaxy group can be generated through the joint action of multiple tidal interactions. About half of S0 galaxies reside in groups (Crook et al. 2007; Wilman et al. 2009). It is possible that tidal interaction is an important mechanism for the formation of S0 galaxies. Future observational studies with bigger sets of samples should reveal a clearer picture of S0 galaxies in groups.

Acknowledgments

We thank the referee for insightful comments that improved the clarity of this manuscript. We acknowledge the support of the National Key R&D Program of China No. 2022YFA1602901. This work is also supported by the National Natural Science Foundation of China (grant Nos. 12373001 and 11933011), and the Central Government Funds for Local Scientific and Technological Development (No. XZ202201YD0020C).

Appendix A
The Kinematics of Two Tidal Tails

To show the kinematics of two tidal tails, we make a velocity-field map, as shown in Figure 6.

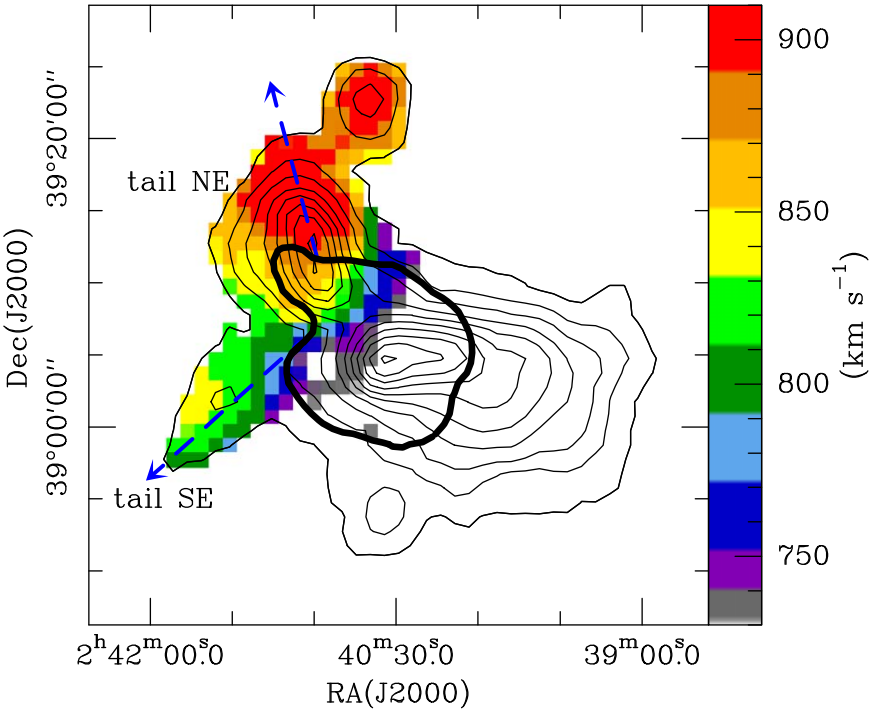

Figure 6. H I velocity-field map in color scale overlaid with the H I column density in the black contours. The velocity ranges from 115 to 295 km s^{-1}. These velocities are relative to the systemic velocity (615 km s^{-1}) of NGC 1023. The thick black line indicates the position and size of NGC 1023A, while the two blue arrows mark the velocity gradients of tail NE and tail SE.

Appendix B
The Kinematics of NGC 1023 in Velocity Space

The PV diagram is often used to describe galactic rotation. Here we utilized the PV diagram to decompose the kinematics of NGC 1023 in velocity space, as shown in Figure 7.

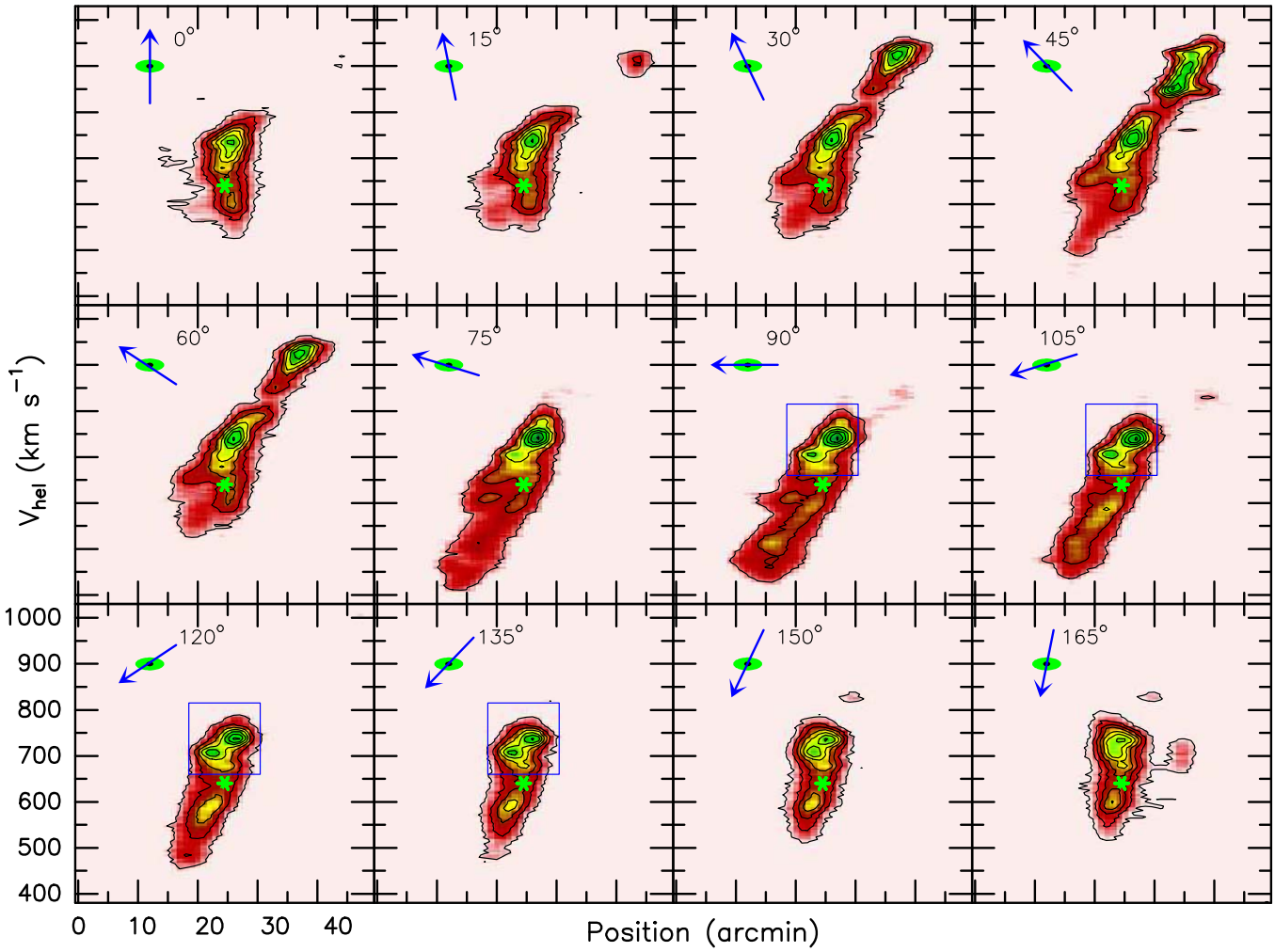

Figure 7. Position–velocity (PV) diagrams, which cut through NGC 1023 along different position angles, shown in blue arrows in the top-left corners of each panel. The blue boxes indicate the binary galaxy, and the green crosses are used to mark the position of S0 galaxy NGC 1023 in the PV diagram.

Appendix C
H I Column Density and Baryonic Mass of the Galaxy

Under the assumption that the gas in galaxies is optically thin for the H I line, the column density $N(x, y)$ in each pixel can be calculated by $N(x, y) = 1.82 \times 10^{18} \int T_B dv$, where dv is the velocity width in km s^{-1}. We made the column-density distribution maps on the obtained moment 0 map (total intensity) using the measured relevant main beam gain T_B/S_ν.

The majority of gas in galaxies is H I and helium. Assuming the same helium-to-H I ratio as that derived from the Big Bang nucleosynthesis, a factor of 1.33 is included to account for the contribution of helium (Planck Collaboration et al. 2020). The baryonic masses (M_{bar}) can be determined by $M_{bar} = M_\star + M_{gas}$, where $M_\star$ is the obtained total stellar mass. The total gas mass of galaxies is derived by $M_{gas} = 1.33 \times M_{HI}$, where M_{HI} is H I gas mass, which can be determined by

$$M_{HI} = 2.36 \times 10^5 D^2 \int S_\nu(x, y) dx dy, \quad \text{(A1)}$$

where D is the adopted distance to each galaxy and $S_\nu(x, y)$ is the integrated H I flux in Jy km s^{-1} in each pixel. Here we take the distance of NGC 1023 as that of each galaxy in this group.

In order to estimate the total stellar mass of each galaxy, we used the Pan-STARRS1 g-band and r-band data. The Pan-STARRS1 survey is a 3π steradian survey with a medium depth in five bands (Chambers et al. 2016). For dwarf galaxies, the stellar mass can be given by Zhang et al. (2017):

$$\log(M_\star/L_g) = -0.745 + 1.616(m_g - m_r), \quad \text{(A2)}$$

where L_g is stellar luminosity in g-band, which can be determined by $L_g = D^2 10^{10-0.4(m_g - M_g^0)}$, where M_g^0 is the absolute solar g-band magnitude, which is adopted as 5.03 mag (Willmer 2018). In order to measure the apparent magnitude (m_g, m_r), we made a new sky-background subtraction of each galaxy using the software SEXtractor (Bertin & Arnouts 1996) and a row-by-row and column-by-column method (Wu et al. 2002; Du et al. 2015). For the starless galaxy NGC 1023E, we can ignore the contribution of stellar mass to the baryonic mass.

Appendix D
Dynamic Masses of the Galaxy

In order to obtain the dynamic mass of the galaxy, we use the Tilted Ring Fitting Code (TiRiFiC) software package to fit its H I cube data. The TiRiFiC is a 3D tilted-ring fitting code that has demonstrated considerable success in describing the kinematics and morphology of rotating disks (Józsa et al. 2007). The Bootstrap method is used to estimate the final values and errors of model parameters. Once we have reached a preliminary final model, we move the individual nodes of the model several times with random values and then restart the fitting process. We calculated the mean and standard deviation of each model parameter after 20 such fitting processes and assumed that the mean is the final model parameter and its error. Apart from the obtained fitting parameters, we also derived model cube data. With the cube data, we created PV diagrams of each galaxy in Figure 8, which can be used to compare with observation data and then determine whether the TiRiFiC model fitting is the best fit. After subtracting the disk model, the residuals are below 3σ significance in Figure 8, where σ is the noise level, suggesting that the majority of the H I gas emission for each galaxy can be modeled as a rotating disk.

Located adjacent to NGC 1023, there are five other galaxies. Since the H I emission size of NGC 1023B and NGC 1023D are smaller ($\leqslant$2 beams), we only successfully fitted the other three relatively large dwarf galaxies. The obtained rotational velocities (V_{rot}) and velocity dispersion (σ_v) from the fittings are listed in Table 1. Because the rotational velocities are comparable with the velocity dispersion for NGC 1023A, NGC 1023C, and NGC 1023E, we need to consider the contribution of velocity dispersion to dynamic mass (Hoffman et al. 1996; Román et al. 2021). We can estimate dynamic mass by $M_{dyn} = (V_{rot}^2 + 3\sigma_v^2) R_{H\,I}/G$, where $R_{H\,I}$ is the effective radius and G is the gravitational constant. To correct for the beam smearing effect, the effective radius can be determined by $R_{H\,I} = \sqrt{D_{H\,I}^2 - B_F^2}/2$, where $D_{H\,I}$ is the uncorrected H I sizes of galaxies, and B_F is the FAST beam size (2.′9). We measured the $D_{H\,I}$ from their H I column-density maps. Observed properties and estimated masses are summarized in Table 1.

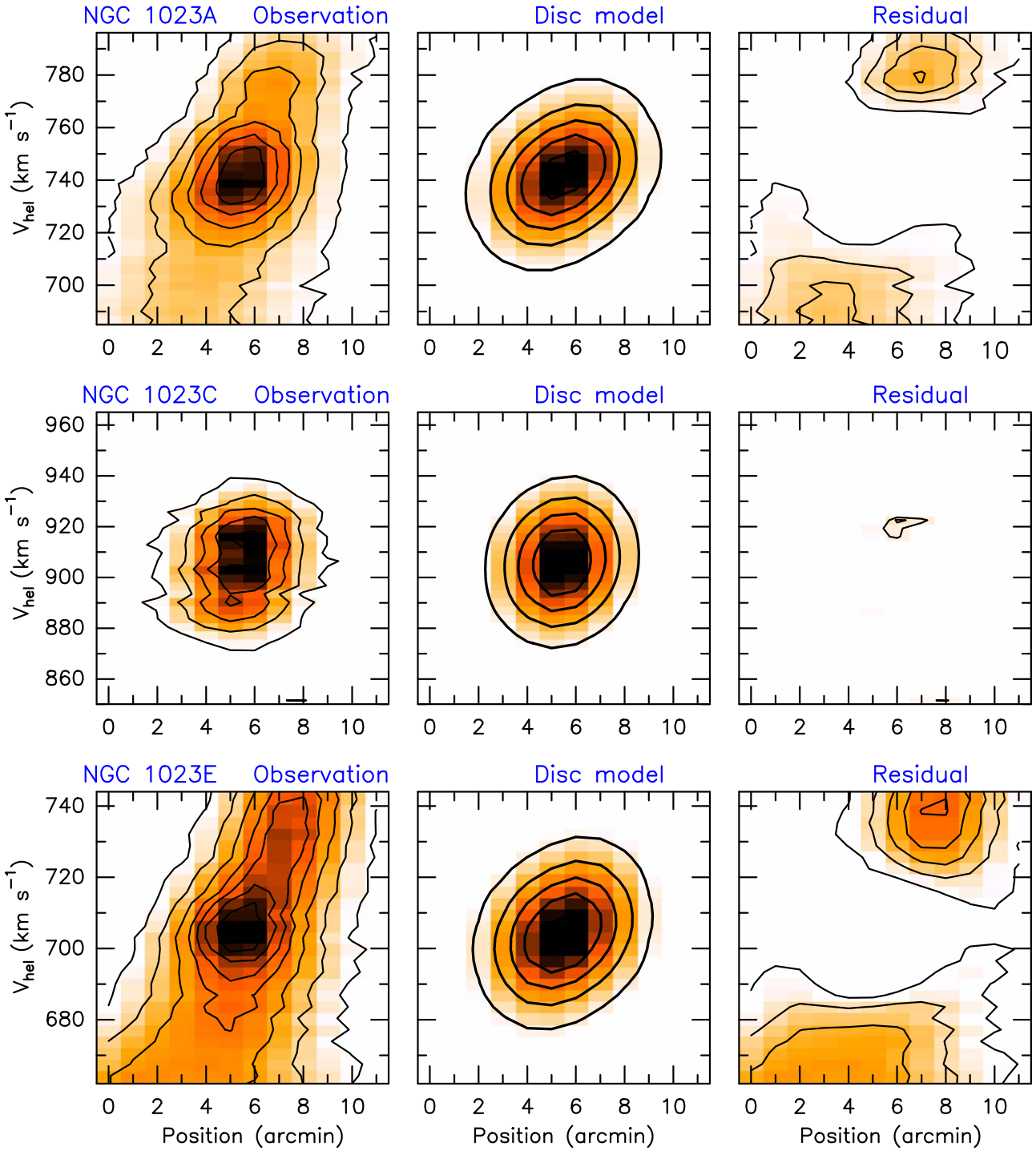

Figure 8. PV diagrams in color scale overlaid with the black contours, obtained from the observed cube (left), model cube (middle), and residual cube (right). The cutting is through the center of each galaxy along their position angles. All the black contours begin at 5σ in each panel. $1\sigma = 1.3$ mJy beam^{-1}.

Table 1
Measured and Derived Properties of the Dwarf Galaxies

Name NGC	R.A. (deg)	Decl. (deg)	V_{sys} (km/s)	i (deg)	V_{rot} (km/s)	σ_v (km/s)	R_{eff} (kpc)	m_g (mag)	m_r (mag)	$\log M_{HI}$ ($M_\odot$)	$\log M_\star$ ($M_\odot$)	$\log M_{dyn}$ ($M_\odot$)	R
1023A	40.1571	39.0575	$740.7^{+0.5}_{-0.5}$	43^{+2}_{-2}	$17.0^{+3.2}_{-3.2}$	$9.3^{+1.5}_{-1.5}$	$20.0^{+1.2}_{-1.2}$	14.29	14.15	$8.4^{+0.1}_{-0.1}$	$8.1^{+0.1}_{-0.1}$	$9.4^{+0.1}_{-0.1}$	$5.6^{+0.4}_{-0.4}$
1023C	40.1650	39.3797	$904.6^{+1.6}_{-1.6}$	81^{+5}_{-5}	$5.1^{+2.9}_{-2.9}$	$11.2^{+1.6}_{-1.6}$	$12.3^{+1.3}_{-1.3}$	17.02	16.59	$7.8^{+0.1}_{-0.1}$	$7.2^{+0.1}_{-0.1}$	$9.1^{+0.1}_{-0.1}$	$11.5^{+1.0}_{-1.0}$
1023E	40.0667	39.0845	$704.2^{+0.7}_{-0.7}$	47^{+3}_{-3}	$12.9^{+3.1}_{-3.1}$	$7.5^{+1.4}_{-1.4}$	$18.7^{+1.1}_{-1.1}$	...	...	$8.3^{+0.1}_{-0.1}$	...	$9.2^{+0.1}_{-0.1}$	$5.5^{+0.6}_{-0.6}$
1023B	40.2500	39.0719	$573.3^{+2.6}_{-2.6}$	...	...	...	...	16.74	16.25	$6.8^{+0.2}_{-0.2}$	$7.4^{+0.1}_{-0.1}$	...	...
1023D	40.1375	38.9003	$699.3^{+1.6}_{-1.6}$	...	...	...	...	16.62	15.97	$7.5^{+0.1}_{-0.1}$	$7.5^{+0.1}_{-0.1}$	...	...

Note. We list: Equatorial coordinates (R.A., Decl.); system velocity (V_{sys}); inclination angle (i); rotational velocity (V_{rot}); velocity dispersion (σ_v); effective radius (R_{eff}); absolute g-band and r-band magnitudes (m_g, m_r); H I gas mass ($M_{H\,I}$); stellar mass ($M_\star$); dynamic mass (M_{dyn}); R is the ratio of the dynamical masses to the baryons masses.

ORCID iDs

Jin-Long Xu https://orcid.org/0000-0002-7384-797X
Ming Zhu https://orcid.org/0000-0001-6083-956X
Kelley M. Hess https://orcid.org/0000-0001-9662-9089
Chuan-Peng Zhang https://orcid.org/0000-0002-4428-3183
Xiao-Lan Liu https://orcid.org/0000-0002-1768-9591
Jie Wang https://orcid.org/0000-0002-9937-2351

References

Baek, S.-J., Park, A., Ahn, Y.-J., et al. 2015, Analyst, 140, 250
Balogh, M. L., Navarro, J. F., & Morris, S. L. 2000, ApJ, 540, 113
Barnes, J. E., & Hernquist, L. 1992, Natur, 360, 715
Bekki, K., & Couch, W. J. 2011, MNRAS, 415, 1783
Bertin, E., & Arnouts, S. 1996, AAS, 117, 393
Bettoni, D., Buson, L., & Mazzei, P. 2000, MNRAS, 423, 2957
Bournaud, F., & Duc, P.-A. 2006, A&A, 456, 481
Bournaud, F., Jog, C. J., & Combes, F. 2005, A&A, 437, 69
Briggs, F. H. 1990, AJ, 100, 999
Broeils, A. H., & Rhee, M. H. 1997, A&A, 324, 877
Capaccioli, M., Lorenz, H., & Afanasjev, V. L. 1986, A&A, 169, 54
Cappellari, M., Emsellem, E., Krajnović, D., et al. 2011, MNRAS, 416, 1680
Chambers, K. C., Magnier, E. A., Metcalfe, N., et al. 2016, arXiv:1612.05560
Coccato, L., Jaffé, Y. L., Cortesi, A., et al. 2020, MNRAS, 492, 2955
Corsini, E. M., Morelli, L., Pastorello, N., et al. 2016, MNRAS, 457, 1198
Cortesi, A., Arnaboldi, M., Coccato, L., et al. 2013, A&A, 549, 115
Cortesi, A., Chies-Santos, A. L., Pota, V., et al. 2016, MNRAS, 456, 2611
Cortesi, A., Merrifield, M. R., Arnaboldi, M., et al. 2011, MNRAS, 414, 642
Crook, A. C., Huchra, J. P., Martimbeau, N., et al. 2007, ApJ, 655, 790
Davies, J. I., Disney, M. J., Minchin, R. F., et al. 2006, MNRAS, 368, 1479
de Brito Silva, D., Coelho, P., Cortesi, A., et al. 2022, A&A, 664, A129
Debattista, V. P., Corsini, E. M., & Aguerri, J. A. L. 2002, MNRAS, 332, 65
Deeley, S., Drinkwater, M. J., Michael, J., et al. 2020, MNRAS, 498, 2372
Deeley, S., Drinkwater, M. J., Michael, J., et al. 2021, MNRAS, 508, 895
Dolfi, A., Forbes, D. A., Couch, W. J., et al. 2021, MNRAS, 504, 4923
Dressler, A. 1980, ApJ, 236, 351
Du, W., Wu, H., Lam, M. I., et al. 2015, AJ, 149, 199
Duc, P. A., Bournaud, F., & Masset, F. 2004, A&A, 427, 803
Forbes, D. A., Almeida, A., Spitler, L. R., & Pota, V. 2014, MNRAS, 442, 1049
Fraser-McKelvie, A., Aragón-Salamanca, A., Merrifield, M., et al. 2019, MNRAS, 481, 5580
Gaia Collaboration, Prusti, T., de Bruijine, J. H. J., et al. 2016, A&A, 595, 1
Gallagher, J. S., III, & Duc, D. A. 1984, ARA&A, 22, 37
García-Ruiz, I., Sancisi, R., & Kuijken, K. 2002, A&A, 394, 769
Gunn, J. E., Gott, J., & Richard, III. 1972, ApJ, 176, 1
Herrmann, K. A., & Ciardullo, R. 2009, ApJ, 705, 1686
Hoffman, G. L., Salpeter, E. E., Farhat, B., et al. 1996, ApJS, 105, 269
Jiang, P., Tang, N.-Y., Hou, L.-G., et al. 2020, RAA, 20, 064
Jiang, P., Yue, Y. L., Gan, H. Q., et al. 2019, SCPMA, 62, 959502
Józsa, G. I. G., Kenn, F., Klein, U., & Oosterloo, T. A. 2007, A&A, 468, 731
Larsen, S. S., & Brodie, J. P. 2002, AJ, 123, 1488
Larson, R. B., Tinsley, B. M., & Caldwell, C. N. 1980, ApJ, 237, 692
Laurikainen, E., Salo, H., Buta, R., et al. 2010, MNRAS, 405, 1089
Lelli, F., Duc, P.-A., Brinks, E., et al. 2015, A&A, 584, 113
Moore, B., Lake, G., & Katz, N. 1998, ApJ, 495, 139
Morganti, R., de Zeeuw, R. T., Oosterloo, T. A., et al. 2006, MNRAS, 371, 157
Noordermeer, E., Merrifield, M. R., Coccato, L., et al. 2008, MNRAS, 384, 943
Planck Collaboration, Aghanim, N., Akrami, Y., et al. 2020, A&A, 641, 6
Rahmani, H., Péroux, C., Augustin, R., et al. 2018, MNRAS, 474, 254
Rizzo, F., Fraternali, F., & Iorio, G. 2018, MNRAS, 476, 2137
Román, J., Jones, M. G., Montes, M., et al. 2021, A&A, 649, L14
Sancisi, R., Fraternali, F., Oosterloo, T., et al. 2008, A&ARv, 15, 189
Sancisi, R., van Woerden, H., Davies, R. D., & Hart, L. 1984, MNRAS, 210, 497
Springel, V., Di Matteo, T., Hernquist, L., et al. 2005, MNRAS, 361, 776
Taylor, E. N., & Webster, R. L. 2005, ApJ, 634, 1067
Tonry, J. L., Dressler, A., Blakeslee, J. P., et al. 2001, ApJ, 546, 681
Toomre, A., & Toomre, J. 1972, ApJ, 178, 623
Toribio, M. C., Solanes, J. M., Giovanelli, R., et al. 2011, ApJ, 732, 93
Trentham, N., & Tully, R. B. 2009, MNRAS, 398, 722
van der Kruit, P. C., & Freeman, K. C. 2011, ARA&A, 49, 301
Westmeier, T., Kitaeff, S., Pallot, D., et al. 2021, MNRAS, 506, 3962
Willmer, C. N. A. 2018, ApJS, 236, 47
Wilman, D. J., Oemler, A., Jr., Mulchaey, J. S., et al. 2009, ApJ, 692, 298
Wu, H., Burstein, D., Deng, Z., et al. 2002, AJ, 123, 1364
Xu, J. L., Zhang, C. P., Yu, N., et al. 2021, ApJ, 922, 53
Zanatta, E. J. B., Cortesi, A., Chies-Santos, A. L., et al. 2018, MNRAS, 479, 5124
Zhang, H. X., Puzia, T., & Weisz, D. R. 2017, ApJS, 233, 12